Journal of Engineering Mathematics, Vol. 4, No. 3, July 1970
Wolters-Noordhoff Publishing–Groningen
Printed in the Netherlands



# A Numerical Investigation of Wake Deformation in Density Stratified Fluids

H. PADMANABHAN, W. F. AMES, J. F. KENNEDY, TIN-KAN HUNG

*Institute of Hydraulic Research, Department of Mechanics and Hydraulics, University of Iowa, Iowa City, Iowa (U.S.A.)*

(Received December 18, 1969)

SUMMARY

The collapse shape and internal velocity field of an initially circular homogeneous fluid mass surrounded by a linearly stratified fluid are computed. During the initial stage of collapse, the fluid is assumed to be irrotational and inviscid while in later stages the Navier–Stokes equations are solved numerically by a modification of Chorin's primitive variable decomposition method. The final stage is analyzed by means of an asymptotic viscous long-wave theory.

## 1. Introduction

Even very mild density stratification in a fluid can radically alter its dynamic behavior and have seemingly disproportionate effects, giving rise to phenomena that are unknown in homogeneous fluids. Such is the case for wakes in density stratified liquids. Whereas wakes in homogeneous fluids of large extent are subjected everywhere to the same gravitational force, the mixing and consequent disruption of the equilibrium density configuration by turbulent wakes in stratified fluids result in gravity induced pressure gradients that generate secondary fluid motions. These motions are responsible for the vertical collapse and horizontal spreading of the wake cross-section, which in turn generate internal gravity waves and horizontal displacement of fluid outside the wake; these phenomena are absent in homogeneous-fluid wakes. The phenomenon of collapse of three-dimensional wakes was first demonstrated by Schooley and Stewart [1], in small-scale experiments with a selfpropelled cylindrical body moving along its axis in a linearly stratified liquid. Schooley and Stewart also pointed out that a collapsing wake is an efficient generator of internal gravity waves, many of which are of high order, that manifest themselves in lateral movement of the fluid at the free surface. Kennedy and Froebel [2] measured the velocity distribution in a wake generated by a two-dimensional plate towed at the interface of a two-layered fluid, and found that the wake half-width (defined as the distance between the points where the velocity is one-half the centerline velocity) attains a maximum a short distance behind the plate, and then rapidly diminishes. Monroe and Mei [3] investigated the shapes of two-dimensional wakes generated by a circular cylinder towed normal to its axis through linearly stratified fluids, and also found that stratification inhibits vertical expansion of the wake and can lead to wake collapse.

The collapse processes are quite different for two- and three-dimensional wakes. In the former, collapse occurs if gravitational forces restore fluid displaced vertically, by turbulent diffusion, to levels of static equilibrium before turbulent mixing relieves the density difference over the region of disequilibrium. Monroe and Mei [3] introduced into the classical differential equation describing two-dimensional wake growth a term to account for the gravitational "restoring force," and were thereby able to predict the general form of the wake growth and subsequent collapse. For three-dimensional wake configurations, on the other hand, the wake (mixed region) initially grows because of turbulent mixing, as is also the case for two-dimensional wakes. However, the ensuing collapse results primarily from the mixed fluid moving toward and spreading laterally at a level where it will be in static equilibrium with the surrounding fluid. The collapse and accompanying lateral spreading produce horizontal displacement of the stratified fluid surrounding the mixed region; the fluid laterally adjacent to the wake converges above and below the level of spreading, and is displaced outward at the level where

the mixed fluid finds density equilibrium, as was noted by Stockhausen, Clark, and Kennedy [4].

Wu [5], [6] conducted a cleverly conceived experimental investigation of an idealized representation of the three-dimensional wake collapse process in a plane normal to the path of the wake-generating body. He isolated, dyed, and thoroughly mixed a semi-circular section of a linearly stratified fluid contained in a long, relatively narrow, laboratory tank. The mixed fluid was then released into the surrounding stratified fluid and its collapse and spreading were recorded photographically. From the motion picture film, Wu was able to obtain precise time records of the fluid deformation. He found that the collapse process can be divided into three stages, which he termed "initial", "principal", and "final". Empirical formulas were obtained to describe the process during the first two stages, and the scaling parameter appropriate to these stages was found to have the form of the Brunt–Väisälä frequency. During the first two phases of the collapse, very little mixing occurred at the interface between the homogeneous and the stratified fluids. The final stage of collapse was complicated by viscous effects and by the onset of mixing at the thin tip of the wake.

The primary objective of the calculation described herein was to develop a computational model for both the shape and internal velocity field of an initially circular homogeneous region surrounded by a linearly stratified liquid of infinite extent. During the initial stage of collapse the fluid is assumed to be inviscid and the motion irrotational. For the later stages, when viscous effects assume a significant rate, the complete Navier–Stokes equations are solved. The final stage of collapse is analyzed by means of a viscous, long-wave theory. The pressure acting on the boundary of the mixed region is assumed to be hydrostatic throughout the collapse process. The computed results are found to be in reasonable agreement with the experimental data obtained by Wu [5], [6] in the corresponding physical model. A new numerical method is described for obtaining solutions for the complete Navier–Stokes equations in problems involving moving boundaries. The technique involves an extension of an approach due to Chorin [7], [8].

## 2. Formulation and Numerical Solution for the Inviscid Model

The coordinate system adopted and the initial configuration to be analyzed are depicted in Figure 1. Note that in the coordinate system chosen, $\rho_y < 0$ for stable static conditions. The

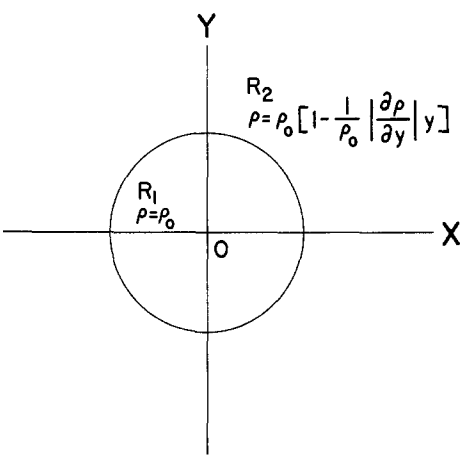


Fig. 1. Definition sketch.

regions interior and exterior to the boundary of the homogeneous (wake) zone are denoted by $R_1$ and $R_2$, respectively. The fluid in $R_1$ is treated as incompressible and inviscid and the motion as irrotational. Hence, the equation to be solved is

$$\nabla^2 \phi = \phi_{xx} + \phi_{yy} = 0 \text{ in } R_1 \tag{1}$$

where $\phi$ is the velocity potential such that

$$u = -\phi_x\,, \quad v = -\phi_y\,. \tag{2}$$

The motion in $R_2$ is largely ignored. The pressure exerted on $R_1$ and $R_2$ is assumed to be the hydrostatic pressure of the stratified fluid. The dynamic boundary condition at the density interface, $y=\eta$, is thus

$$-\phi_t - g\frac{\rho_y}{\rho_0}\frac{y^2}{2} + \tfrac{1}{2}(u^2+v^2) = 0 \text{ on } y=\eta\,. \tag{3}$$

The kinematic boundary condition on the boundary of $R_1$ will be satisfied automatically in the numerical scheme used to calculate the boundary motion. The homogeneous region, $R_1$, is assumed to be initially circular with diameter $D_0 = 2a_0$ and at rest; hence, the initial conditions are

$$\left.\begin{aligned} u = v = 0 \\ x^2+\eta^2 = a_0^2 \end{aligned}\right\} \text{ at } t=0\,. \tag{4}$$

If the equations set forth above are non-dimensionalized using $D_0$, $\rho_0$, $(g|\rho_y|/\rho_0)^{-\frac{1}{2}}$, and $D_0^2 g|\rho_y|$ as the characteristic length, density, time, and pressure, respectively, they retain exactly the same form in the dimensionless variables. Furthermore, it emerges that $D_0|\rho_y|/\rho_0$ is the dimensionless parameter characterizing the problem.

The computational philosophy is as follows. The dynamic boundary conditions on $\eta$, (3), is expressed in a forward difference form,

$$[\phi(t+\Delta t)-\phi(t)]_{y=\eta} = \Delta t\left\{-g\frac{\rho_y}{\rho_0}\frac{y^2}{2} + \frac{u^2+v^2}{2}\right\}_{y=\eta;\,t} + O[(\Delta t)^2] \tag{5}$$

For the static initial conditions described by (4),

$$\phi(\Delta t)|_{y=\eta} = -\Delta t\left\{g\frac{\rho_y}{\rho_0}\frac{y^2}{2}\right\}_{y=\eta;\,t=0} + O[(\Delta t)^2]\,. \tag{6}$$

Equations 5 and 6 give the boundary values of $\phi$ at any time $t+\Delta t$. The velocity potential at interior points, at $t+\Delta t$, was determined from a finite difference simulation of (1).

The Gauss–Seidel method, accelerated by the successive overrelaxation schemes described by Young [9] and given in Ames [10], was used to obtain $\phi$. Preliminary computational experiments revealed that the convergence rate of this method for the present problem is at least four times as great as that of the standard Gauss–Seidel iteration. After $\phi$ was determined for each interior mesh point, the interior velocities were calculated by numerical differentiation and the boundary velocities were obtained from interior velocities by three- or five-point Lagrangian extrapolation. The boundary velocities so obtained were used to calculate the position of the density interface at the end of the time increment, and were also substituted into (5) to obtain the boundary values for calculation of $\phi$ at $t+2\Delta t$. The double symmetry of the initial boundary and of the initial boundary condition, (6), assures that the boundary contour and velocity field will be bisymmetric, about the $x$ and $y$ axes, at all subsequent times; consequently, the finite difference calculation was carried out only for one quadrant. Symmetry also dictated that the boundary conditions along $OY$ and $OX$ (see Figure 1) are $\phi_x = 0$ and $\phi_y = 0$, respectively. The domain of integration was subdivided into a rectangular grid. The vertical and horizontal increments were both initially taken to be equal to $D_0/24$. Later, as the boundary deformed, their magnitudes were changed independently as needed to reduce the convergence time. The computational molecules were modified as needed at meshes cut by the curvilinear boundary, due attention being given to maintaining consistent computational accuracy. The convergence criterion adopted was $|\Delta\phi|/\phi \leqq 0.001$ between successive trials. A dimensionless time increment of $\Delta t = 0.2$ was chosen after some preliminary computational experimentation.

As an independent check on the computational scheme, the Dirichlet problem for the initial circular profile was solved by use of Poisson's integral formula, and the results compared with

those obtained by the method of finite differences. The solutions were indistinguishable.

A more complete description of the calculational strategy and details is given by Padmanabhan [11] in his doctoral thesis. Suffice it here to note that the finite-difference scheme was adopted in preference to a variational method or one involving integral equations because most of the computational framework utilized in the finite difference scheme was also required for the viscous model. A comparison of the computational results with available experimental data is presented in Section 5.

## 3. Formulation and Numerical Solution for the Viscous Model

The model described in the preceding section can be expected to describe the collapse process only during the early stages, when the momentum balance is primarily between gravitational and inertial effects. Later, as the velocity and velocity gradients develop, dissipative forces play an even greater role. If the viscosity, either molecular or eddy, is assumed to be constant in time and space—a tenuous but practically unavoidable assumption—the non-dimensionalized equations to be treated are

$$u_x+v_y=0 \tag{7}$$

$$u_t+uu_x+vu_y=-\frac{1}{F^2}h_x+\frac{1}{R}\nabla^2 u \tag{8}$$

$$v_t+uv_x+vv_y=-\frac{1}{F^2}h_y+\frac{1}{R}\nabla^2 v \tag{9}$$

where $h=p/\rho_0 g+y$ is the piezometric head, $F^2=D_0|\rho_y|/\rho_0$, $R=(\rho_0 D_0^2\sqrt{g|\rho_y|/\rho_0})/\mu$, and $\mu$ denotes the viscosity—molecular or other. The collapse process is now characterized by two dimensionless groupings, the additional one reflecting the role of viscosity.

The kinematic boundary condition will be automatically fulfilled in the computational model, as it was for the inviscid case, since after each discrete time interval the boundary displacement is computed from the boundary velocities. The dynamic boundary conditions require that the normal and tangential stresses be continuous across the interface. These conditions are difficult to satisfy exactly for several reasons. First, the normal stress can be calculated only if the surface orientation is known; however, this can be accurately sensed in a finite difference approximation only if the mesh is very fine. Second, and more important, in the iteration scheme used, various velocity derivatives at the surface were chosen on the basis of (7), but these do not necessarily give the correct viscous stresses. Finally, since the motion of the fluid in $R_2$ was not calculated, it was not known what shear stress is applied to the boundary. In view of these difficulties, the lead of Harlow and Welch [12] was followed, the viscous stresses on the interface were ignored, and the surface pressure equated directly to the hydrostatic pressure of the surrounding stratified fluid. This should be an adequate measure, except in cases of very small values of $R$.

The numerical solution of incompressible viscous flow problems presents some formidable difficulties, due mainly to the special role played by pressure gradients. In two-dimensional problems, this difficulty can be by-passed by eliminating the pressure from the equations and treating vorticity and the stream function as the pertinent dependent variables. Unfortunately, the vorticity stream function technique could not be used to good advantage in the present problem because the interface is not a streamline. Therefore, it was decided to seek solutions of the governing equations in the primitive variables: the velocity and piezometric head. The bisymmetry made it possible to limit the domain of solution to one quadrant.

The numerical methodology adopted is an extension of one recently developed and employed by Chorin [7], [8]. Let $u$, $v$ and $h$ denote the solution of (7), (8), and (9) as well as their discrete approximations, and let $DV=0$ be a difference approximation for the continuity equation, (7). It is assumed that at time $t=n\Delta t$, velocity and piezometric head fields $u^n$, $v^n$, and $h^n$ are given

satisfying $DV^n=0$. The task at hand is to evaluate $u^{n+1}$, $v^{n+1}$, and $h^{n+1}$ using the governing equations so that $DV^{n+1}=0$.

Auxiliary fields $F_1(u, v)$ and $F_2(u, v)$ are computed by means of

$$u^{aux} = u^n + \Delta t F_1(u, v) \tag{10}$$

$$v^{aux} = v^n + \Delta t F_2(u, v) \tag{11}$$

where

$$F_1(u, v) = -uu_x - vu_y + \frac{1}{R}\nabla^2 u \tag{12}$$

and

$$F_2(u, v) = -uv_x - vv_y + \frac{1}{R}\nabla^2 v\,. \tag{13}$$

It can be seen that in the evaluation of $u^{aux}$ and $v^{aux}$, the piezometric head terms in the Navier–Stokes equations have not yet been included. A variant of the alternating direction scheme analyzed by Samarskii [13] is used to evaluate $u^{aux}$ and $v^{aux}$ from (10)–(13). The initial conditions on $(u, v)$ are given by the velocity field at $t=n\Delta t$. On the $x$-axis, $\partial u/\partial y=0$ but $\partial v/\partial y\neq 0$. The contribution of the term $\Delta t F_1(u, v)$ of Eq. (10), at points on the $x$-axis, is shown to be small compared to $u^n$ by Padmanabhan [11]. As the wake elongates the significance of the term further decreases. Chorin [8] also employs the boundary conditions adopted herein on the $x$-axis, namely $u^{aux}=u^n$, $\partial u^{aux}/\partial y|_{y=0}=0$.

The piezometric head is now calculated. The divergence of the Navier–Stokes equation is approximated by the finite difference analogue

$$\frac{1}{F^2} Lh^n = -\frac{DV^n}{\Delta t} - DQV^n + \frac{1}{R} DLV^n \tag{14}$$

where $DV$ approximates $\nabla \cdot V$, $LV$ approximates $\nabla^2 V$, $Q$ approximates $V\cdot\nabla V$ and $L$ approximates $\nabla^2 h$. The first term on the right-hand side of (14) arises because of Chorin's [7], [8] numerical method. Equation (14) is a Poisson equation in $(h)$, and was solved iteratively by employing a five point computational molecule and a Dufort–Frankel relaxation scheme (Ames, [14]) using the auxiliary velocities calculated according to (10) and (11). For the present problems, the values of the piezometric head are known on the curvilinear boundary. Symmetry properties were used on the coordinate axes.

Written in detail, the implicit Dufort–Frankel scheme takes the following form at an interior point ($u_{i,j}^{n,m}=u^m(i\Delta x, j\Delta y, n\Delta t)$, $m$ the iteration number)

$$h_{i,j}^{n+1,m+1} = h_{i,j}^{n+1,m} - F^2\lambda\left[(u_{i+1,j}^{n+1,m+1} - u_{i-1,j}^{n+1,m+1})/2\Delta x + (v_{i,j+1}^{n+1,m+1} - v_{i,j-1}^{n+1,m+1})/2\Delta y\right]$$

$$u_{i+1,j}^{n+1,m+1} = u_{i+1,j}^{aux} - \frac{1}{F^2}(\Delta t/2\Delta x)\left[h_{i+2,j}^{n+1,m} - \tfrac{1}{2}(h_{i,j}^{n+1,m} + h_{i,j}^{n+1,m+1})\right]$$

$$u_{i-1,j}^{n+1,m+1} = u_{i-1,j}^{aux} - \frac{1}{F^2}(\Delta t/2\Delta x)\left[\tfrac{1}{2}(h_{i,j}^{n+1,m+1} + h_{i,j}^{n+1,m}) - h_{i-2,j}^{n+1,m}\right]$$

$$v_{i,j+1}^{n+1,m+1} = v_{i,j+1}^{aux} - \frac{1}{F^2}(\Delta t/2\Delta y)\left[h_{i,j+2}^{n+1,m} - \tfrac{1}{2}(h_{i,j}^{n+1,m+1} + h_{i,j}^{n+1,m})\right]$$

$$v_{i,j-1}^{n+1,m+1} = v_{i,j-1}^{aux} - \frac{1}{F^2}(\Delta t/2\Delta y)\left[\tfrac{1}{2}(h_{i,j}^{n+1,m+1} + h_{i,j}^{n+1,m}) - h_{i,j-2}^{n+1,m}\right].$$

The quantity $\lambda$ is analogous to the successive over-relaxation parameter $\omega$ and the direct relationship between them is given by

$$\omega = 2/\left[1 + (\tfrac{1}{2}\lambda)(\Delta x^2/\Delta t)\right].$$

Modifications near the boundaries are discussed in detail by Padmanabhan [11].

Two major difficulties were encountered in the computation. The first occurred when the intersections of the curvilinear boundary with the grid lines were used as the mesh points for the finite difference analysis. This approach did not consistently produce convergent results, probably because some of the mesh distances adjacent to the boundary were very small. The problem was resolved by approximating the partial differential equations with the standard finite difference molecule at all points. As a consequence, the boundary conditions were satisfied not on the curvilinear boundary, but on an exterior ring of meshpoints of polygonal shape.

The second problem was more serious. During the process of computation, it was found that the finite difference scheme behaved well when the shape of the boundary is circular, or nearly so. At later times, when the shape became elongated, the scheme diverged because there were not enough meshpoints near the wake tip to define a finite difference approximation to the prescribed order of accuracy. Two alternative solutions were considered. The first was to use a mesh size in the vertical direction which is much smaller than that in the horizontal direction. Second, the mesh size could be kept the same in both directions, but the problem solved in a transformed, nearly circular region. Such a transformation could be accomplished by linearly stretching all the vertical dimensions. After some numerical experimentation, the latter alternative was found to be superior and hence was adopted.

Such a linear transformation requires transformation of the governing equations and boundary conditions as well. In order that the transformed equations retain, so far as possible, the same form as the original equations, the vertical velocity and the piezometric head were also stretched by means of the relations

$$y^T = \beta y, \quad v^T = \beta v, \quad h^T = \beta h$$

where $\beta$ is a magnification parameter and superscript $T$ denotes the transformed variable. The transformed counterparts of (7), (8), and (9) are:

$$u_x + v^T_{y^T} = 0 \tag{15}$$

$$u_t + uu_x + v^T u_{y^T} = -\frac{1}{\beta F^2} h^T_x + \frac{1}{R}(u_{xx} + \beta^2 u_{y^T y^T}) \tag{16}$$

$$v^T_t + uv^T_x + v^T v^T_{y^T} = -\frac{\beta}{F^2} h^T_{y^T} + \frac{1}{R}(v^T_{xx} + \beta^2 v^T_{y^T y^T}). \tag{17}$$

Equations 15–17 are written in finite difference forms, in which they retain almost the same form as the original equations, and solved subject to the transformed initial and boundary conditions. After the iterative processes were completed, the transformed variables were reconverted to the original variables. Since the whole intention was to work with a more or less circular boundary, the magnification parameter $\beta$ was modified as the profile changed; $\beta$ was initially unity and in the final stages became as large as twelve.

Even though the behavior of the finite difference scheme was improved with this modification, it still had some shortcomings. For example, the convergence, which was very fast during the early stages, became rather slow at large times. This necessitated termination of the computational solution at approximately ten dimensionless time units.

A value of 0.2 was chosen for $\Delta t$. It was found that if $(u\,\Delta t)$ and $(v\,\Delta t)$ are both much smaller than unity, no instability difficulties are present. If, however, the values of the horizontal or vertical velocity reach values such that either $u\Delta t$ or $v\Delta t$ exceeds about 0.10, the iterative scheme for the determination of auxiliary velocities becomes unstable. There are no theoretical guidelines for determining spatial mesh sizes required for a specified error. After some preliminary trials, the initial mesh size was taken as $D_0/16$. The convergence criterion adopted was $\Delta h/h \leqq 0.002$. The two values of the Reynolds number, $R$, employed in this study, were very high: 50.000 and 70.000. The numerical scheme did not present any difficulties on this account. A comparison of the computational results with available experimental data will be given in Section 5.

## 4. Asymptotic Solution for the Final Stage of Decay

At large times after the initiation of motion, when the boundary between $R_1$ and $R_2$ becomes very elongated, a long-wave approximation suitable for viscous fluids should be applicable*. Let it be assumed that the flow is then locally horizontal and only weakly time dependent. In other words, the physical unknowns, $u$ and $p$, are slowly varying functions of $x$ and $t$. Therefore, if dimensional variables are restored, the Navier–Stokes equations reduce to

$$\mu u_{yy} = p_x, \qquad 0 < y < \eta \,. \tag{18}$$

The motion remains symmetric with respect to both axes. Assuming now that the pressure distribution in both the fluids is hydrostatic, the pressures $p_1$ in the inner fluid and $p_2$ in the outer fluid are

$$p_1 = \rho_0 g(\eta - y) + p_2|_{y=\eta} \tag{19}$$

$$p_2 = p_0 - \int_0^y \rho_0 g(1 + y\rho_y/\rho_0)dy \,. \tag{20}$$

Upon substituting (20) and (19) and differentiating with respect to $x$, there results

$$\frac{1}{\rho_0} p_{1_x} = -g(\rho_y/\rho_0)\eta\eta_x \,. \tag{21}$$

Hereinafter, the subscript 1 is dropped and $p$ denotes the pressure in the inner fluid. Introduction of (21) and (18) yields

$$u_{yy} = \alpha(x, t) \tag{22}$$

where $\nu$ is the kinematic viscosity of the inner fluid and $\alpha = -(g\rho_y/\nu\rho_0)\eta\eta_x$. Since the dependent variables are assumed to be only slowly varying functions of $x$ and $t$, direct integration is possible so that

$$u = \frac{\alpha y^2}{2} + \bar{B}y + \bar{C} \tag{23}$$

where $\bar{B}$ and $\bar{C}$ are integration constants. Since the motion is symmetric with respect to the $x$-axis, $\bar{B} = 0$. Moreover, the maximum velocity occurs at the centerline; therefore

$$u = \frac{\alpha y^2}{2} + u_{\max} \,. \tag{24}$$

Inspection of the computational results obtained from the inviscid model for $t > 15$ (dimensionless units), when the hydrostatic pressure distribution is valid, revealed that the ratio of the horizontal velocity at the interface to that at the centerline is primarily a function of $(x/a(t))$, where $a(t)$ is the wake front position, and that this function can be closely approximated by an equation of the type

$$\frac{u(\eta)}{u_{\max}} = \frac{\xi + A}{B\xi + C} \tag{25}$$

where $A$, $B$ and $C$ are constants, and $\xi = x/a(t)$. The computational result, from the inviscid solution, and the approximation (given by (25)) with $A = -0.05$, $B = 0.90$, and $C = 0.05$, are shown in Figure 2. (In Mei's analysis, cited above, it was assumed that the ratio $u/u_{\max}$ is constant.) Substitution of (25) into (24) yields

$$u = \frac{\alpha}{2}\left(y^2 - \frac{\eta^2}{1 - \dfrac{\xi + A}{B\xi + C}}\right). \tag{26}$$

* This approach was suggested by an analysis performed by Professor C. C. Mei [15] of the MIT Hydrodynamics Laboratory and sent to Kennedy as a personal communication.

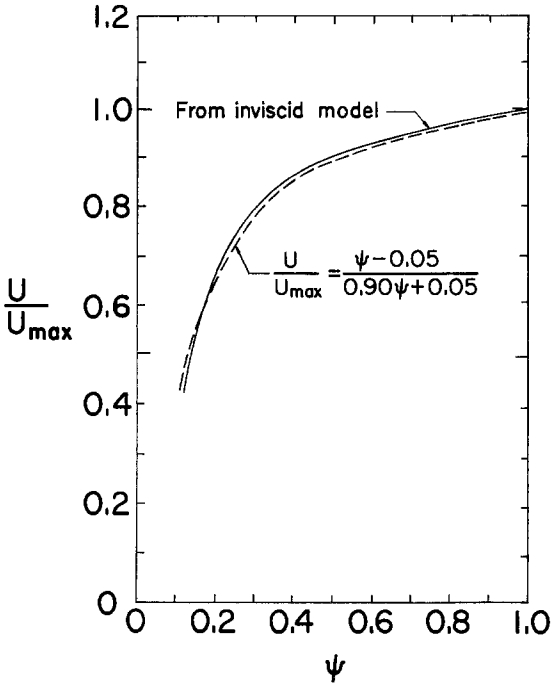


Fig. 2. Ratio of horizontal velocity at density interface to velocity at midheight ($y=0$), computed from inviscid model and approximated by polynomial.

The discharge per unit width through the upper half of the layer, $0<y<\eta$, is obtained by integrating (26):

$$q=\int_0^{\eta} u\,dy=\frac{\eta^3\alpha}{2}\left(\tfrac{1}{3}-\frac{1}{1-\dfrac{\xi+A}{B\xi+C}}\right). \tag{27}$$

Substituting (27) into the continuity equation, $q_x+\eta_t=0$, yields

$$\eta_t+\frac{\partial}{\partial x}\left[\frac{\eta^3\alpha}{2}\left(\tfrac{1}{3}-\frac{1}{1-\dfrac{\xi+A}{B\xi+C}}\right)\right]=0. \tag{28}$$

The mathematical formulation will be more convenient if the solution is sought in the $(\xi, t)$ plane. In the new variables, (28) becomes

$$\eta_t+\frac{g}{2va^2}\frac{\rho_y}{\rho_0}\frac{\partial}{\partial\xi}\left[\left(\frac{1}{1-\dfrac{\xi+A}{B\xi+C}}-\tfrac{1}{3}\right)\eta^4\eta_\xi\right]=0. \tag{29}$$

Equation (29) is similar to the $q$-dimensional equation with spherical symmetry, discussed by Ames [14]. Since the similarity variable is $x/a(t)$, a trial solution is attempted in separated form:

$$\eta(\xi, t)=T(t)\cdot X(\xi) \tag{30}$$

with $T$, $X$ and $a$ as yet unspecified. Substitution of (30) into (29) yields

$$T^5\left(-\frac{g}{2v}\frac{\rho_y}{\rho_0}\right)\frac{\partial}{\partial\xi}\left[\left(\frac{1}{1-\dfrac{\xi+A}{B\xi+C}}-\tfrac{1}{3}\right)X^4X'\right]=a(t)[aT'X-\xi TX'a'] \tag{31}$$

where the primes denote differentiation. The right-hand side of (31) may be expressed as

$$a(t)\begin{vmatrix} X & \xi X' \\ Ta' & T'a \end{vmatrix}$$

which is separable if and only if

$$Ta' = -DT'a \tag{33}$$

where $D$ is a constant. Integration of (33) gives

$$a = T^{-D}. \tag{34}$$

The right-hand side of (31) takes the form $a^2 T'(X + D\xi X')$ so that the equation separates to

$$a^2 \frac{T'}{T^5} = -\frac{g}{2v}\frac{\rho_y}{\rho_0} \frac{\dfrac{d}{d\xi}\left[\left(\dfrac{1}{1-\dfrac{\xi+A}{B\xi+C}} - \tfrac{1}{3}\right)X^4 X'\right]}{X + D\xi X'} = -E. \tag{35}$$

The continuity condition is now expressible as

$$\int_0^a \eta\, dx = aT\int_0^1 X\, d\xi = \frac{\pi a_0^2}{4} \tag{36}$$

where $a_0$ is the radius of the initial circular profile. Since $\int_0^1 X\, d\xi$ is a constant, $aT$ is also a constant, and from $a(t) = T^{-D}$ it follows that $D = 1$ and $aT = 1$. Introduction of this information into (35) yields the relation

$$\frac{T'}{T^7} = -E$$

which upon integration becomes

$$T = [6(Et - F)]^{-\frac{1}{6}} \tag{37}$$

where $F$ is a constant of integration. Since $aT = 1$, it follows that

$$a = [6(Et - F)]^{+\frac{1}{6}}. \tag{38}$$

Introducing $D = 1$ into (35) and integrating once with respect to $\xi$ yields

$$\frac{g}{2v}\frac{\rho_y}{\rho_0}\left[\frac{1}{1-\dfrac{\xi+A}{B\xi+A}} - \tfrac{1}{3}\right] X^4 X' = E\xi X + G \tag{39}$$

where $G$ is an integration constant. Since $X' = 0$ when $\xi = 0$, $G = 0$. With this condition, (39) can be cast into the form

$$X^3 X' = \frac{2vE}{g}\frac{\rho_0}{\rho_y} \frac{\xi}{\left[\dfrac{1}{1-\dfrac{\xi+A}{B\xi+C}} - \tfrac{1}{3}\right]}. \tag{40}$$

Integration once again with respect to $\xi$ yields

$$X = \left\{\frac{-24vE}{g}\frac{\rho_0}{\rho_y}\right\}^{\frac{1}{4}} \left\{-\frac{B-1}{(2B+1)}\frac{\xi^2}{2} - \left[(C-A) - \frac{(2C+A)(B-1)}{(2B+1)}\right] \times \left[\frac{\xi}{2B+1} - \frac{2C+A}{(2B+1)^2}\log_e\left(\xi + \frac{2C+A}{2B+1}\right)\right] + H\right\}^{\frac{1}{4}} \tag{41}$$

where $H$ is a constant of integration that can be expressed in terms of $A$, $B$, and $C$ through use of the condition $X(1)=0$. Since $a_0$ and $\rho_0/\rho_y$ are known quantities, the constant $E$ can be evaluated by substituting (41) into (36).

The other constant of integration in (37) and (38), $F$, has to be evaluated from the initial conditions. The condition at $t=0$ is not applicable since many of the assumptions used in the long-wave analysis are not then valid. Instead, the initial condition was taken as the computed value of the wake-front coordinate at $t$ equal to about fifteen dimensionless units. Knowing $T(t)$ and $X(\xi)$, the form of the profile at any time can be found from (30). The velocity of the wake front can be obtained by differentiating (38),

$$u(a(t)) = E[6(Et-F)]^{-\frac{5}{6}}.$$

A comparison of the results with experimental data is furnished in the following section.

## 5. Comparison of Computational and Experimental Results

Calculations were carried out for density gradients of $-\rho_y/\rho_0=0.01549$ and $0.0807\ \text{ft}^{-1}$ for the inviscid model and $-\rho_y/\rho_0=0.01549$ and $0.00810\ \text{ft}^{-1}$ for the viscous models. These conditions correspond to three of those included in the experimental investigation conducted by Wu [5], described briefly in Section 1. The kinematic viscosity, $\nu$, was taken to be $1.2\times10^{-5}$ $\text{ft}^2/\text{sec}$. Figure 3 presents a comparison for one density gradient between the measured wake

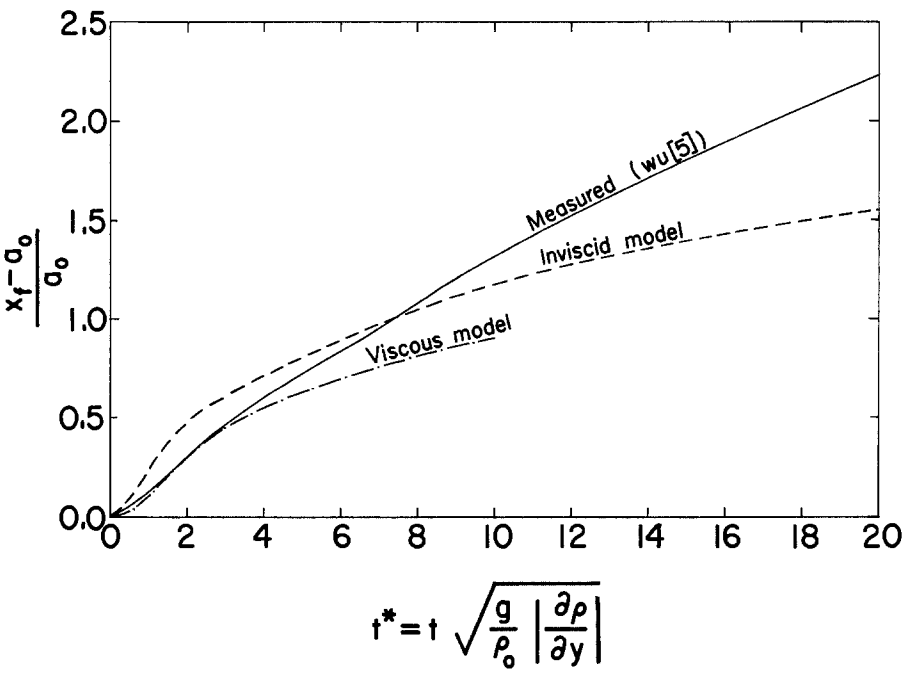


Fig. 3. Observed and computed values of lateral wake-front position, as functions of non-dimensionalized time: $(1/\rho_0)|\partial\rho/\partial y|=0.01549\ \text{ft}^{-1}$.

front advance and those calculated using the inviscid and viscous finite difference models. The choice of the particular value of $\rho_y/\rho_0$ is somewhat inconsequential, inasmuch as Wu found that the data for $t<\sim25$, for all density gradients studied, fell along one curve when plotted in the format of Figure 3. The agreement between the measured values and those computed using the viscous model is acceptable for values of non-dimensional time $t$ less than about 5; thereafter, there is pronounced divergence. The discrepancy at larger $t$ arises, no doubt, from the assumption of hydrostatic pressure in the stratified fluid. In fact, the pressure applied to the homogeneous zone must be significantly affected by the motion in $R_2$, and in such a way

that the spreading occurs faster than calculated. Additionally, Wu's [5] Figure 9 shows that there is an apparently minor instability at the density interface that causes the formation of minor advance fronts above and below the level of principal spreading. The present model does not allow for such instability. Additional sources of divergence are the finite size of the tank used by Wu, and the errors arising from round-off, truncation, and discretization errors arising in the numerical solution. Logarithmic plots of the computed data presented in Figure 3 revealed that $a/a_0$ varies as $t^{0.33}$ and $t^{0.31}$ for the inviscid and viscous models, respectively. Wu [5] found in his experimental study that $a/a_0 = 1.03\ t^{0.55}$ during the principal stage of collapse ($4 < t < 25$).

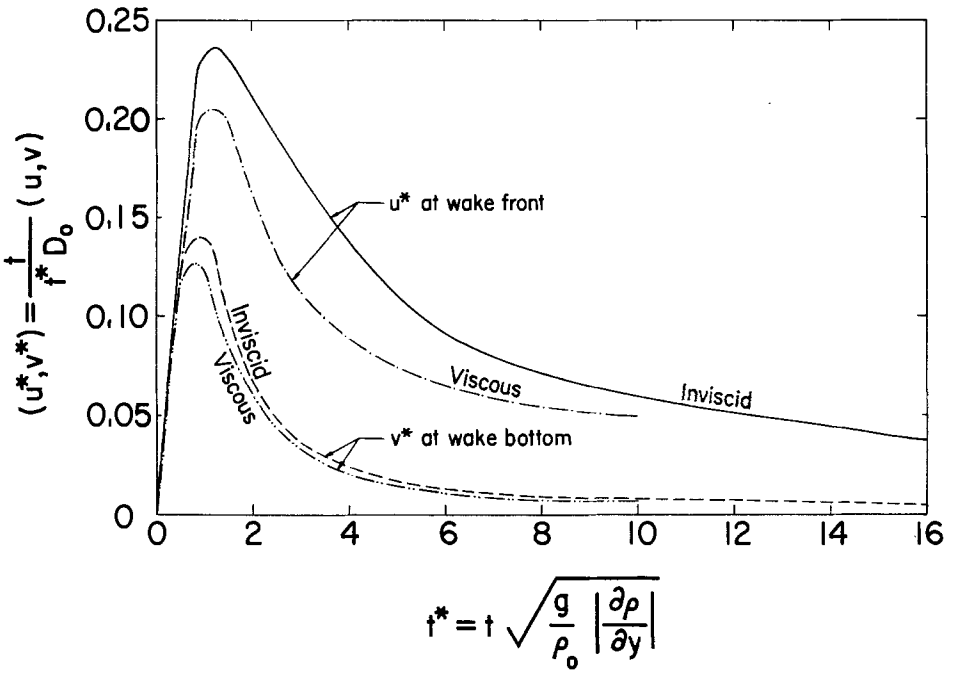


Fig. 4. Horizontal velocities at wake front and vertical velocities at wake bottom computed with inviscid and viscous models. $(1/\rho_0)|\partial\rho/\partial y| = 0.01549\ \text{ft}^{-1}$.

Figure 4 depicts the computed horizontal velocities at the wake front and vertical velocities at the wake apogee (or perigee) as functions of dimensionless time. It is seen that both velocities rapidly attain maxima and then diminish. The velocities computed with the viscous and inviscid models exhibit quite similar behavior throughout the period covered by the calculation.

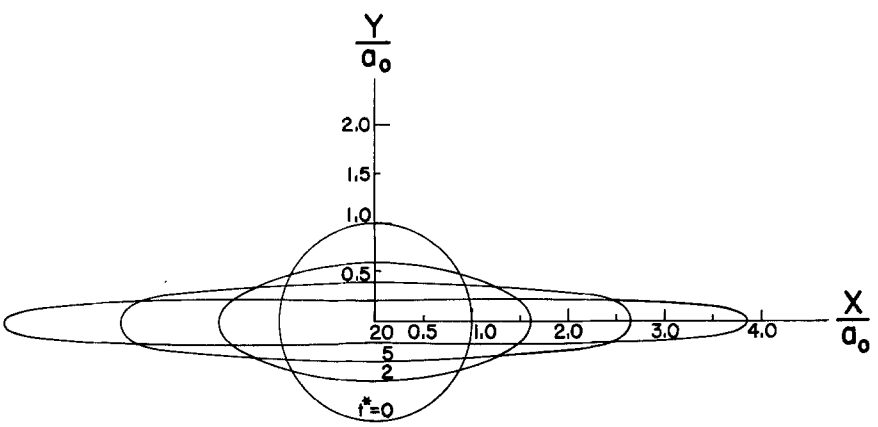


Fig. 5. Wake profiles at various non-dimensionalized times, computed using inviscid model. $(1/\rho_0)|\partial\rho/\partial y| = 0.01549\ \text{ft}^{-1}$.

Figure 5 shows the wake contours computed with the inviscid model. The corresponding results obtained with the viscous model were found to be very similar in qualitative character, and exhibit the quantitative differences the data of Figure 3 would indicate. As a loose check on the computational procedure, the area of the profile was evaluated at each computational time step and compared to the initial area of the mixed region; the difference never exceeded five per cent of the area of the initial circle.

The long-wave formulation for the final stage of decay was evaluated for the two density gradients specified above. A summary comparison of computed and measured wake front

TABLE 1

*Comparison between calculated and measured wake front positions*

| $t\left(\frac{\lvert\rho_y\rvert}{\rho_0}g\right)^{\frac{1}{3}}$ | $a(t)/a_0$ (calculated) | $a(t)/a_0$ (measured by Wu (1965)) |
|---|---|---|
| | $-\rho_y/\rho_0 = 0.01549\ \text{ft}^{-1}$ | |
| 17.7 | 7.60 | 6.00 |
| 35.4 | 10.50 | 8.20 |
| 70.7 | 12.10 | 10.20 |
| | $-\rho_y/\rho_0 = 0.00810\ \text{ft}^{-1}$ | |
| 12.8 | 5.00 | 5.00 |
| 35.6 | 9.20 | 7.20 |
| 51.1 | 11.04 | 10.20 |

positions is presented in Table 1. The dimensional formulas obtained after evaluating the constants $E$ and $F$ in Eq. (38) are, in ft/sec units,

$$a(t) = [6(120t - 2500)]^{\frac{1}{6}}, \quad -\rho_y/\rho_0 = 0.01549\ \text{ft}^{-1}$$

and

$$a(t) = [6(62t - 1500)]^{\frac{1}{6}}, \quad -\rho_y/\rho_0 = 0.00810\ \text{ft}^{-1}.$$

At large $t$ ($t > 100$ sec, say), the second term in parenthesis becomes negligible and $a \approx t^{\frac{1}{6}}$, and the wake front velocity varies as $t^{-\frac{5}{6}}$. Note that results obtained with the viscous model, used to evaluate the initial condition, are influenced by the inertial, gravitational, and viscous effects, and hence it is not possible to express $a(t)$ as a function of just one scaling parameter during the final stage of collapse.

Additional computational results, including distributions of velocities and piezometric head, are presented by Padmanabhan [11] in his thesis.

**Acknowledgements**

Financial support for this study was provided by the Office of Naval Research, United States Navy, under contract NR-062-053. The cost of much of the computer time was borne by the Graduate College of The University of Iowa.

REFERENCES

[1] A. H. Schooley and R. W. Stewart, Experiments with a self-propelled body in a fluid with a vertical density gradient, *J. Fluid Mech.* 15 (1963) 83–96.

[2] J. F. Kennedy and R. A. Froebel, Two-dimensional turbulent wakes in density stratified fluids, *ASME* Pub. 69-WA/UNT-N.

[3] R. H. Monroe and C. C. Mei, *The shape of two-dimensional turbulent wakes in density-stratified fluids*, M.I.T. Hydrodynamics Lab. Rept. No. 110, 1968.

[4] P. J. Stockhausen, C. B. Clark and J. F. Kennedy, *Three-dimensional momentumless wakes in density-stratified liquids*, M.I.T. Hydrodynamics Lab. Rept. No. 93, 1966.

[5] J. Wu, *Collapse of turbulent wakes in density-stratified media*, Hydronautics Inc. Tech. Rept. 231–4 (1965).

[6] J. Wu, *Wake collapse and subsequent generation of internal waves in a density-stratified medium*, Hydronautics Inc. Tech. Rept. 231–17 (1968).
[7] A. J. Chorin, *The numerical solution of the Navier–Stokes equations for an incompressible fluid*, AEC Research and Development Rept. No. NYO-1480-82, New York University, 1967.
[8] A. J. Chorin, Numerical solution of the Navier Stokes equations, *Maths. Comp.*, 22 (1968) 745–762.
[9] D. M. Young, "Iterative methods for solving partial difference equations of elliptic type", *Trans. Amer. Math. Soc.* 76 (1954) 92–111.
[10] W. F. Ames, *Numerical Methods for Partial Differential Equations*, Thos. Nelson and Sons, London; Barnes and Noble, New York (1969).
[11] H. Padmanabhan, *Wake Deformation in Density-Stratified Fluids*, Ph.D. Dissertation, University of Iowa (1969).
[12] F. H. Harlow and J. E. Welch, Numerical calculations of time-dependent viscous incompressible flow of fluid with free surface, *Phys. of Fluids*, 8 (1963) 2182–2189.
[13] A. A. Samarskii, An efficient difference method for solving a multidimensional parabolic equation in an arbitrary region, *U.S.S.R. Comp. Math. and Math. Phys.*, 5 (1963–1964) 894–926.
[14] W. F. Ames, *Nonlinear Partial Differential Equations in Engineering*, Academic Press, New York, 1965.
[15] C. C. Mei, *Collapse of a Homogeneous Fluid Mass in a Stratified Fluid*, 12th International Congress of Applied Mechanics, Stanford University, Stanford, Calif., Aug. 26–31, (1968).